ORIGINAL PAPER

Moisture absorption and spectroscopic studies of epoxy clay nanocomposite

K. Muralishwara[1] · **Y. N. Sudhakar[2]** · **U. Achutha Kini[1]** · **Sathyashankara Sharma[1]** · **B. M. Gurumurthy[1]**

Abstract

Epoxy resins are prone to serious moisture absorption inspite of their inherent advantages, which can be mitigated by the incorporation of montmorillonite nanoclay that provide tortuous path to flow of moisture. Moisture absorption studies of epoxy clay nanocomposites is carried out, to analyse the effect of nanoclay content, immersion media and immersion temperature. Nanocomposites prepared in 0.5, 1 and 1.5 wt% using magnetic stirring and ultrasonication and neat epoxy specimen were immersed in distilled water and artificial seawater maintained at 28 and 38 °C till saturation. Fick's and Langmuir's models were applied to calculate the kinetic parameters from the water absorption graphs. Atomic force microscopy (AFM), X-ray diffraction spectroscopy (XRD), Fourier transform infrared spectroscopy (FTIR) and scanning electron microscope with energy dispersive X-ray (SEM–EDX) characterizations were performed. Diffusivity is least for nanocomposite containing 0.5 wt% nanoclay at both temperatures in both medium. However, it is least when the medium is distilled water. As the temperature of immersion medium increases, the diffusivity also increases. Saturation moisture uptake increased with increase in nanoclay content, because of the residual hydrophilic nature of nanoclay. AFM and XRD analysis revealed better dispersion and exfoliated structure of nanoclay respectively at 0.5 wt% loading. FTIR spectroscopy was applied to identify the chemical bonds that helped in proposing the reaction mechanism of the nanocomposite synthesis. Spectra comparison of dry and wet specimens complimented the moisture absorption data by showing lower infrared transmittance in wet specimens. With Increase in nanoclay content, the transmittance decreased corresponding to increase in saturation moisture uptake for distilled water immersed specimens. SEM–EDX analysis distinguished between the cations entered from the artificial seawater and cations that were still present in the nanoclay.

Keywords Epoxy clay nanocomposites · Fourier transform infrared spectroscopy · Moisture diffusion · Fick's law · Langmuir model

---

Extended author information available on the last page of the article

Introduction

Corrosion of marine structures is a serious problem since it results in 30% of the total equipment failure [1]. Organic polymer coatings can mitigate this problem by being a passive barrier between external environment and underlying metallic substrate. Among such class of materials, epoxy resins have been utilized in a wide range of applications due to their excellent adhesion strength, thermal stability, high mechanical properties, chemical resistance, and low shrinkage [2]. However, epoxy resins are vulnerable to moisture absorption, due to which degradation of structure can take place. To reduce or delay the moisture absorption and hence increase the life of epoxy coatings, incorporation of nano-clay as a secondary phase has attracted the attention of many researchers due to the torturous path it provides to the passage of moisture or any other corrosive species [3]. Nanoclay due to its unique shape and high aspect ratio can tremendously improve barrier properties [4, 5]. Among nanoclays, montmorillonite is most used due to its 2D-structure, high aspect ratio and large surface area [6].

When cured epoxy is exposed to or immersed in water at elevated temperatures, the hygrothermal aging can cut the backbone of epoxy chains and products leach out [7]. In coating applications in immersion conditions, water can enter and saturate the epoxy film which lead to reduction of adhesion strength [8]. Epoxy-amine networks when hydrothermally aged, can fail due to various mechanisms such as plasticization, chain scission, thermo-oxidation, residual curing, leaching, polymer relaxation, etc. [9].

When montmorillonite was incorporated in epoxy used for aircraft radome applications, the moisture absorption behaviour of epoxy nanocomposites changed dramatically. The addition of surface modified montmorillonite to epoxy resin in 2 wt%, enhanced the radome performance and longevity by delaying a 16% in relative permittivity by 760 h [10]. Surface modification of nanoclay using organic modifier is important to make it compatible with organic polymer and thereby increase the *d*-spacing. When different organically modified montmorillonite nanoclays at 2 wt% was experimented on water barrier performance of epoxy nanocomposite, Nanomer 1.30E and Cloisite 10A containing epoxy nanocomposites showed 60% reduction in diffusivity [11]. When organo-modified montmorillonite nanoclay was added in 1, 3 and 5 wt% to epoxy, as the amount of added nanoclay increased, maximum water uptake decreased. However, diffusion coefficient reduced by 18% for 1 wt% nanoclay addition, increased by 1.2% when nanoclay was increased from 1 to 3 wt% and again reduced by 18.5% when nanoclay content was increased from 3 to 5 wt%. The lowest diffusion coefficient value was registered for epoxy nanocomposite containing 5 wt% nanoclay. There are few studies on water absorption of epoxy clay nanocomposite, however no studies were found on artificial seawater absorption. Also, a comprehensive study considering the effect of immersion medium, immersion temperature, use of different theoretical diffusion models and application of Fourier transform infrared (FTIR) spectroscopy is scarce.

Marine structures coated with epoxy or structures manufactured by nanocomposites are exposed to water for long durations, during which moisture is

absorbed to an extent that depends on chemical composition, morphology, and degree of curing. Fourier transform infrared (FTIR) spectroscopy is a non-destructive way of identifying the chemical species and bond types present in a material by assigning specific wavenumbers to different peaks. Material when exposed to infrared light spectrum vibrate covalent bonds of various molecules resulting in specific absorption or transmission of energy. When specific wave-number results in vibration of a molecule, peaks in the spectra are obtained which can be assigned to the corresponding molecules. The technique can be carried out on samples in the forms of liquids, solutions, pastes, powders, films, fibers, and gases. It is quite rapid, accurate and relatively sensitive [12]. It is also a useful to measure the impact of water absorption on the transmittance of infrared light in polymer nanocomposites and to identify the chemical bonds thereby helping in determining the reaction mechanisms. The main objective of this paper is to study the effect of surface modified montmorillonite nanoclay on the distilled water and artificial seawater moisture absorption behaviour of epoxy nanocomposite by using the absorption or the gravimetric data. To theoretically study the behaviour, two different theoretical models are used – Fick's and Langmuir's model. The specimens were characterized using advanced research instruments such as Atomic force microscopy (AFM), X-ray diffraction (XRD), FTIR spectroscopy and Scanning Electron Microscope with Energy Dispersive X-ray (SEM–EDX).

Experimental details

Materials and processes

Epoxy resin used in the research is Araldite LY556, which is a clear and pale-yellow colour medium viscous unmodified epoxy resin based on bisphenol-A. The curing agent used is Aradur HY951, which is a low viscous aliphatic amine. The resin and curing agent combination is a solvent-free room temperature curing system which are mixed in ratio 10:1 part by weight. The matrix system exhibits good mechanical strength, resistance to atmosphere and chemical degradation. Technical specifications about the chemicals used is listed in Table 1. The montmorillonite nanoclay used was the surface modified one to have a larger d-spacing and better compatibility with the organic polymer matrix. The nanoclay was surface modified by 0.5–5 wt% aminopropyltriethoxysilane and 15–35 wt% octadecylamine and was procured from Merck India pvt. Limited.

Table 1 Technical specification of resin and curing agent system

Property	Unit	Araldite LY556	Aradur HY951
Viscosity at 25 °C	mPa.S	10,000–12,000	10–20
Density at 25 °C	gm/cc	1.15–1.20	0.97–0.99
Flash point	°C	> 200	> 180

The nanocomposite was synthesized by magnetic stirring and ultrasonication [13, 14]. Prior to magnetic stirring, to reduce the viscosity of epoxy resin and thereby improve the dispersion, the resin was heated to a temperature of 50 °C. Magnetic stirring was carried out for 3 h at 850 RPM during which the nanoclay was added gradually. The mixture was then ultrasonicated for 30 min at 75% amplitude. Curing agent was then added, and the mixture was stirred using a hand stirrer in such a way that air bubbles do not evolve, followed by pouring it into the mold of size 20 mm × 20 mm × 2 mm. The nanoclay was added in different concentrations; 0 wt% in the case of neat epoxy and 0.5, 1, and 1.5 wt% in the case of nanocomposites.

Methods

Atomic force microscopy (AFM)

The surface morphology and topography of the cured samples (neat epoxy, epoxy clay nanocomposites with 0.5 and 1 wt% nanoclay) were determined using Bruker's Innova AFM device in tapping mode. The extent of dispersion of nanoclay in epoxy and surface roughness of the cured samples were analysed using the technique. Roughness parameters, viz. roughness average (R_a), root mean square (R_q), and maximum height of the profile (R_z) of the cured samples were measured and analyzed. The equations for these three parameters are explained in literature elsewhere [15]. samples of size 1 cm × 1 cm were cut from bigger moulded samples.

X-ray diffraction (XRD)

X-ray diffraction measurements were carried out using a Malvern pananalytical empyrean X-ray diffractometer setup in transmission mode with copper Kα radiation ($\lambda = 1.5406Å$), under a voltage of 45 kV and a current of 40 mA. Scans were acquired in continuous mode over a 2θ range of 2–10° with a step size of 0.013.

Fourier transform infrared spectroscopy (FTIR)

Fourier transform infrared spectra were recorded using Shimadzu IRspirit spectrometer that comes with single reflection ATR accessory for direct measurements without samples having in pellet form. Measurements were carried out in the range of 400–4000 cm^{-1} in transmittance mode.

Immersion testing

The prepared specimen of different composition was immersed in test tubes containing artificial seawater and distilled water. Artificial seawater was prepared as per ASTM D1141-98 standard. The immersion test was carried out as per ASTM D570 standard. Specimens in the test tubes were immersed in water bath which was maintained at two different temperatures 28 and 38 °C. Specimens were removed from test tubes

periodically, wiped off using a soft tissue paper and was weighed using an electronic scale of accuracy 0.001 gm. Moisture uptake, M_t at any time during immersion was calculated using Eq. (1) as [16].

$$M_t(\%) = \frac{W_t - W_o}{W_o} \times 100 \tag{1}$$

where W_t is mass at time t and W_o is initial mass of the specimen.

Graph of M_t/M_∞ versus $\sqrt{t}$ was plotted, and Fick's Law (Eq. 2) was numerically fit to the experimental data using least squares approach to determine diffusion coefficient 'D'. Langmuir model (Eq. 3) was also used to numerically fit the experimental data obtained for all the specimens. The two models are compared with respect to their accuracy in fitting the data points or they are used to address the cases where the Fick's law does not fit the experimental data accurate enough due to anomalous behavior. MATLAB curve fitting application was used to numerically fit the models to the experimental data. The adjusted R-square values, Sum of Squared Errors (SSE) and Root Mean Square Error (RMSE) values obtained after fitting are provided along with graphs.

$$\frac{M_t}{M_\infty} = \left[1 - \sum_0^\infty \frac{8}{(2n+1)^2 \pi^2} \exp\left(\frac{-D(2n+1)^2 \pi^2 t}{4l^2} \right) \right] \tag{2}$$

$$\frac{M_t}{M_\infty} = 1 - \frac{\gamma}{\gamma + \alpha} e^{-xt} - \frac{8}{\pi^2} \frac{\alpha}{\alpha + \gamma} \sum_0^\infty \frac{1}{(2n+1)} \times \exp\left[-\left(\frac{\pi(2n+1)}{2l} \right)^2 Dt \right] \tag{3}$$

In Eqs. (1)–(3), M_∞ is moisture uptake at saturation, n is number of terms, D is diffusion coefficient in mm²/hr., t is time in hr., 2 l is specimen thickness in mm. In Eq. (3), γ is probability of mobile molecules getting bound and α is probability of bound molecules becoming mobile.

Scanning electron microscope with energy dispersive X-ray (SEM–EDX)

Scanning electron microscope (EVO MA18) with Oxford EDS(X-act) was used to identify the nanoclay present in the epoxy and the salts in the artificial seawater that diffused into the specimen. The immersed specimen was cut in required size and were gold sputtered before testing. Neat epoxy and epoxy clay nanocomposite with 1.5 wt% nanoclay was chosen for the testing. Specifically, nanocomposites with lower nanoclay loadings were not chosen, owing to the fact that trace elements and elements low in concentrations cannot be accurately detected using EDX analysis.
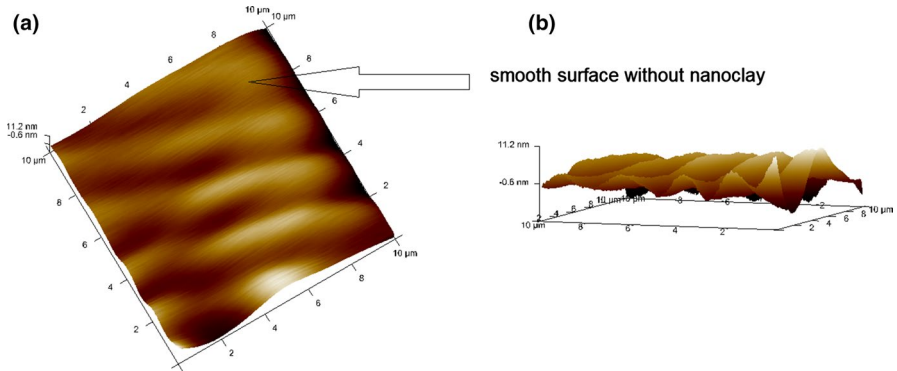
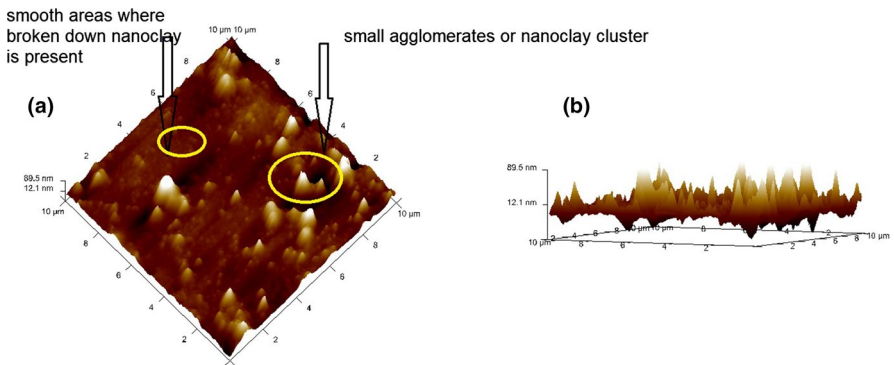**Fig. 1** Atomic force microscope images showing the **a** surface and **b** height profile

Fig. 2 AFM images of epoxy clay nanocomposite with 0.5 wt% nanoclay showing **a** surface **b** height profile

Results and discussion

Atomic force microscope analysis

The Figs. 1, 2, 3 show the topography image of neat epoxy and epoxy clay nano-composites. The surface roughness parameters obtained from AFM scanning are tabulated in Table 2. Figure 4 show the phase images of neat epoxy and epoxy clay nanocomposites. In topographic images, the brighter areas represent peaks and darker areas represent lower heights or troughs. In phase images, the brighter areas represent presence of nanoclay and darker areas represent the epoxy polymer.

From topography image i.e., Fig. 1a, it is observed that the surface of neat epoxy is smoother and from phase images i.e., Fig. 4a, it is observed that the surface is devoid of any nanoclay. The absence of nanoclay is the reason for the smoothness [17]. From Fig. 1b, it is observed that even though the surface is smooth, there are still some crests and troughs on the surface in nanoscale. The surface roughness
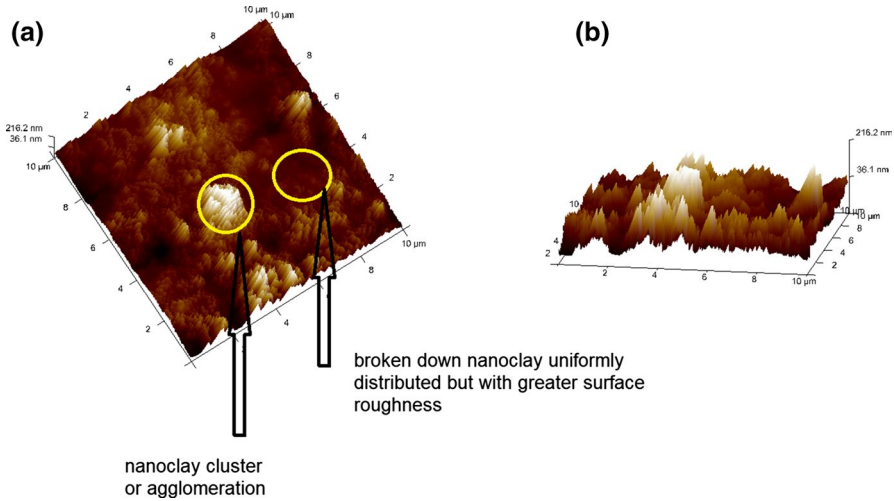
Fig. 3 AFM images of epoxy clay nanocomposite with 1 wt% nanoclay showing **a** surface **b** height profile

Table 2 surface roughness parameters for neat epoxy and epoxy clay nanocomposites

	Average surface roughness R_a	Root mean square surface roughness R_q	$R_q - R_a$	Maximum surface roughness R_{max}
Neat epoxy	2.32	2.98	0.66	22.06
Epoxy clay nanocomposite (0.5 wt% nanoclay)	11.25	16.4	5.15	203.5
Epoxy clay nanocomposite (1 wt% nanoclay)	53.25	72.05	18.8	632

values in the form of three different parameters are given in Table 1. R_a is 2.32 and R_q is 2.98. R_q is mathematically higher than R_a since the higher R_q value represents the standard deviation and are squared. However, the difference between R_q and R_a is 0.66 which is small enough to suggest that there is not much undulation in the neat epoxy. Therefore, the crests and troughs observed is miniscule and hence the surface is uniform and smooth [18].

From Fig. 2a, it is observed that with the addition of 0.5 wt% nanoclay, the surface is rougher when compared with the surface of neat epoxy. The roughness values are 11.25 (R_a) and 16.4 (R_q). The difference of 5.15 between R_a and R_q is approximately 8 times greater than that of neat epoxy. This indicates the presence and distribution of nanoclay on the surface. Nanoclay have tendency to migrate to the surface, resulting in higher roughness in certain areas when compared with area where roughness is that of the matrix or area further away from the nanoclay.
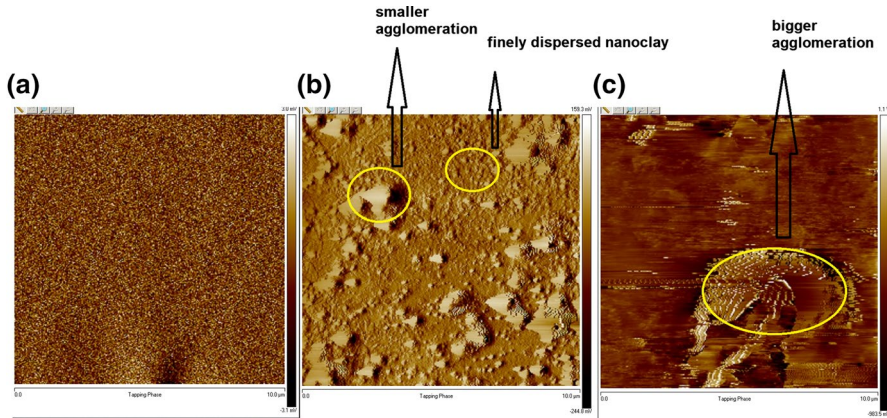
Fig. 4 AFM phase images of **a** neat epoxy **b** epoxy nanocomposite with 0.5 wt% nanoclay and **c** epoxy nanocomposite with 1 wt% nanoclay

Therefore, the difference between R_a and R_q is greater here [17–19]. From Fig. 4b, it is observed that nanoclay is uniformly distributed with small size agglomeration here and there.

From Fig. 3a, it is observed that surface is generally rougher in most of the areas and in some other areas, the roughness is even higher. When compared with 0.5 wt% addition, it is seen that the roughness has generally increased because of higher amount of nanoclay. From the phase image in Fig. 4c it is observed that the size of agglomerations has also increased since the chances of forming agglomerations are higher at higher loading of nanoclay.

X-ray diffraction analysis

Figure 5 presents XRD spectra of organomodified montmorillonite nanoclay (Nanomer 1.31PS) and epoxy clay nanocomposite with nanoclay content 0.5 and 1 wt%. A diffraction peak assigned to the [001] lattice spacing of nanoclay at $2\theta = 4.006°$, corresponds to d-spacing of 2.204 nm. Upon incorporation of nanoclay in epoxy resin, for nanocomposite containing 0.5 wt% nanoclay, there are not any visible peaks observed, which indicates exfoliated structure of nanoclay in epoxy. However, at 1 wt% of nanoclay, peak of very low intensity is observed which indicates intercalated structure. Since the intensity is very low relative to the baseline, it can be concluded that nanoclay is beginning to take up mixture of intercalated and exfoliated structure.

Fourier transform infrared spectroscopy (FTIR) analysis

Figure 6 presents the FTIR spectra of nanoclay, wherein the wavenumber assigned to peaks are labelled. Peak at 454 and 515 cm^{-1} are assigned to Si–O bending and Al–O stretching vibrations respectively [20], Peak at 799 cm^{-1} is assigned to
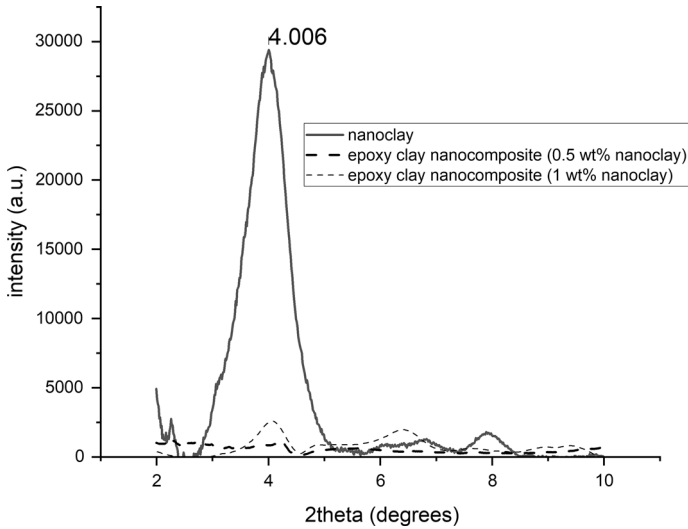
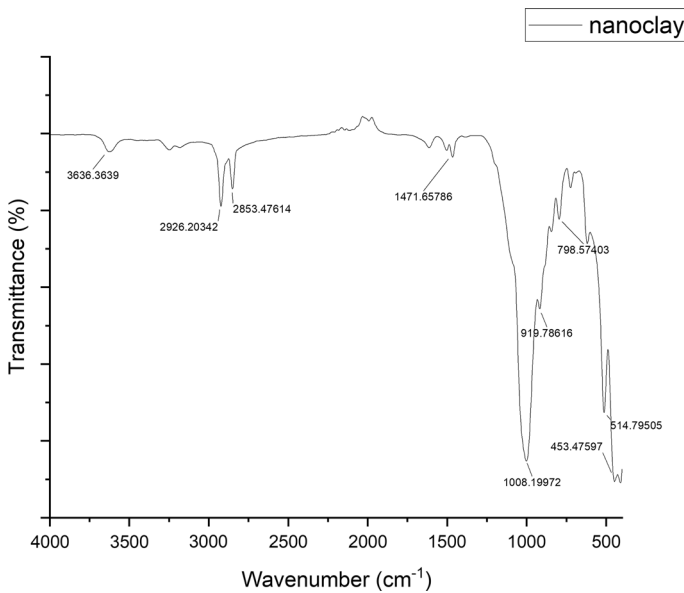**Fig. 5** XRD spectra of nanoclay and epoxy clay nanocomposites

Fig. 6 FTIR spectra of nanoclay

symmetrical stretching vibrations of Si–O–Al [21], peak at 920 cm^{-1} s assigned to AlAlOH bending vibrations [22], peak at 1008 cm^{-1} is assigned to in-plane Si–O–Si stretching vibrations [23], peak at 1472 cm^{-1} is assigned to in-plane scissoring vibrations of C–H [22]. Peaks at 2854 and 2926 cm^{-1} are assigned to C–H

symmetric and asymmetric stretching of surface modifiers of nanoclay respectively [24]. The band at 3636 cm^{-1} is assigned to asymmetric stretching vibration of structural hydroxyl groups present in the nanoclay [25].

Figure 7 presents FTIR spectra of epoxy clay nanocomposites before immersion stacked one over the other. Epoxy resin while curing opens the epoxide ring to form O–H group. The sharp peak at 550 cm^{-1} is assigned to out of plane vibration of O–H and peaks at 760 and 828 are assigned to C–H out of plane vibration [26]. The C–O–C bond stretching of ester groups is assigned to 1228 cm^{-1} [27]. The peak at 1034 cm^{-1} belongs to Si–O–R, assigned to asymmetric Si–O–C stretching in nanoclay, peaks at 1108, 1182 and 1301 cm^{-1} are assigned to C–H in plane bending and the peak at 1462 cm^{-1} is assigned to C–H deformation of CH$_2$ [26]. Peak at 1507 cm^{-1} [28] is assigned to vibration of aromatic ring in DGEBA. The peak at 1611 cm^{-1} [29] is assigned to C=C stretching of aromatic ring. The peak at 2932 cm^{-1} is assigned to asymmetrical C–H stretching of CH$_2$. The peak at 2966 is assigned to asymmetrical C–H stretching CH$_3$ and peak at 2865 cm^{-1} is assigned to aldehyde C–H stretching [26].

Reaction mechanism and scheme of preparation of epoxy clay nanocomposite

The probable reaction mechanism in Fig. 8 shows that the amine group in the hardener Aradur HY951 breaks the epoxy ring of Araldite LY556 and form a crosslinked epoxy resin [30]. The surface modifiers of nanoclay Nanomer 1.31PS, long chain octadecylamine and (3-aminopropyl)triethoxysilane were able to increase the space between the nanoclay layers by dispersing and covalently bonding, respectively [31]. When crosslinked epoxy resin is mixed with surface modified nanoclay, there is enhancement in the crosslinking in the nanoclay matrix [32]. Furthermore, these
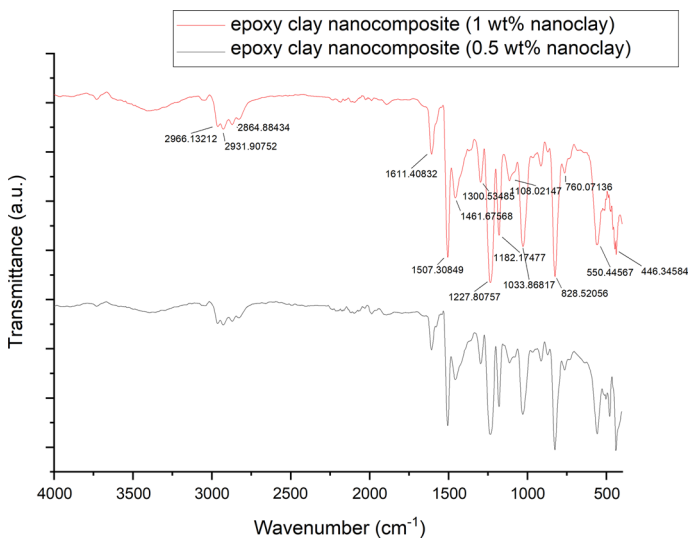

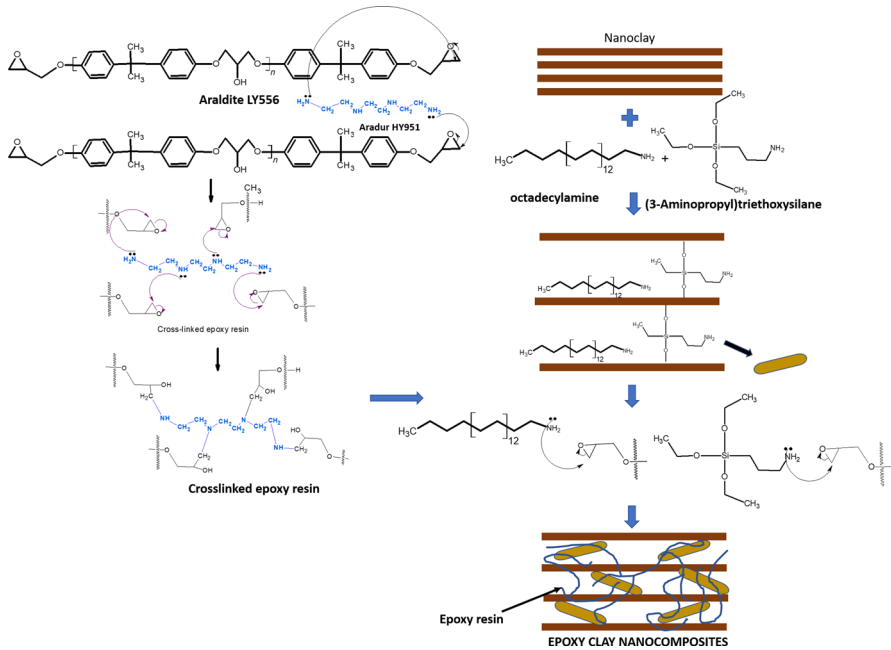**Fig. 7** FTIR spectra of epoxy clay nanocomposites

Fig. 8 Reaction mechanism and scheme of preparation of epoxy clay nanocomposite

surface modifiers of nanoclay containing amine group links with free epoxy chain via breakage of epoxy ring. Hence, surface modifiers help the crosslinked epoxy resin to strongly adhere and get dispersed in the nanoclay matrix.

Moisture absorption studies on epoxy and epoxy clay nanocomposites at 28 °C

The moisture absorption behavior of neat epoxy and epoxy clay nanocomposites when immersed in distilled water at 28 °C is shown in Fig. 9, wherein the scatter plot of M_t/M_∞ versus $\sqrt{t}$ is numerically fit by Fick's law. The diffusion coefficient obtained by curve fitting and saturation moisture uptake obtained from experimentation are given in Table 3. Adjusted R-square, Sum of squares error (SSE) and Root mean square error (RMSE) values are given in Table 4. From Fig. 9, it is observed that the experimental data approximately follows Fick's law. The R-square, SSE and RMSE values indicate that the model satisfactorily fits the experimental data with minimum error.

The diffusion coefficient obtained by curve fitting using least squares approach is highest for nanocomposites containing 1.5 wt%, followed by nanocomposite containing 1 wt% nanoclay and neat epoxy. Lowest value of diffusion coefficient is recorded for epoxy clay nanocomposite containing 0.5 wt% nanoclay. The diffusion coefficient increases when nanoclay is added beyond 0.5 wt% because of nanoclay agglomeration. The agglomeration can also be called as intercalated structure,
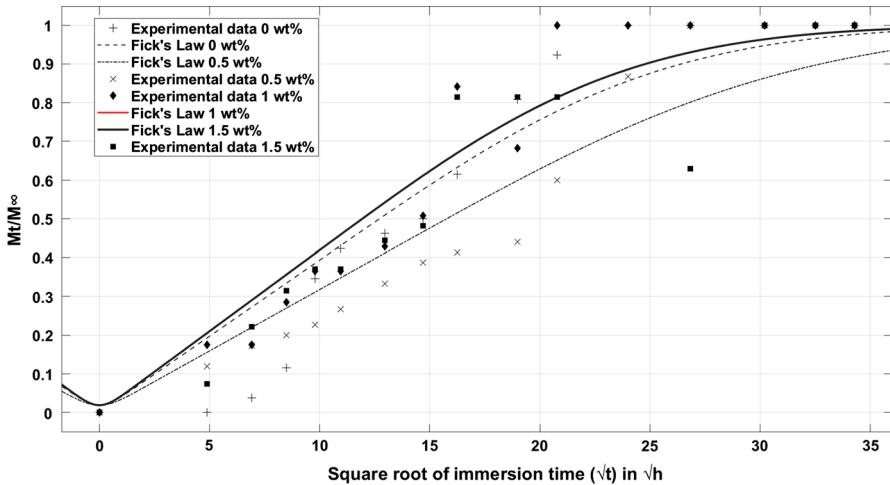
Fig. 9 Experimental data scatter plot of M_t/M_∞ versus $\sqrt{t}$ of samples immersed in distilled water at 28 °C along with Fick's law

Table 3 Diffusion coefficient obtained by Fick's Law curve fitting and saturation moisture uptake obtained from experimentation

	Diffusion coefficient (mm²/s) × 10⁷		Saturation moisture uptake	
	Distilled water	Artificial seawater	Distilled water	Artificial seawater
Neat epoxy	0.65	0.86	1.27	2.02
Epoxy clay nanocomposite (0.5 wt% nanoclay)	0.46	0.72	1.45	0.97
Epoxy clay nanocomposite (1 wt% nanoclay)	0.81	1.16	1.80	1.29
Epoxy clay nanocomposite (1.5 wt% nanoclay)	0.85	0.77	1.60	1.73

which was evident from AFM and XRD results. Similar trend was observed in some of the literatures [33, 34].

The saturation moisture uptake is least for neat epoxy and highest for epoxy clay nanocomposite containing 1 wt% nanoclay. The saturation moisture uptake is higher for nanocomposites because the nanoclay remain hydrophilic to some degree even though its surface is organo-modified. Montmorillonite nanoclay are by themselves hydrophilic due to the presence of cations between their surface layers. These cations are exchanged by surface modifiers such as alkyl ammonium salts [6, 35] and aminosilanes [35] to make montmorillontite nanoclay organophilic. This process increases the *d*-spacing in nanoclay and physically swells it and helps in getting exfoliated nanostructure in polymers such as epoxy. However, since there is some hydrophilicity left behind in the nanoclay, distilled water does not directly enter the polymer but into nanoclay, stays and interacts with the cations there and then moves into the polymer and so on [36, 37]. Therefore, because of this phenomenon, when

Table 4 Adjusted R square, SSE and RMSE values obtained after Fick's Law curve fitting

	Adjusted R-square		SSE		RMSE	
	Distilled water	Artificial seawater	Distilled water	Artificial seawater	Distilled water	Artificial seawater
Neat epoxy	0.83	0.82	0.47	0.52	0.17	0.18
Epoxy clay nanocomposite (0.5 wt% nanoclay)	0.89	0.94	0.22	0.12	0.12	0.09
Epoxy clay nanocomposite (1 wt% nanoclay)	0.89	0.90	0.24	0.17	0.12	0.11
Epoxy clay nanocomposite (1.5 wt% nanoclay)	0.82	0.96	0.40	0.06	0.16	0.07

nanoclay increases from 0.5 to 1 wt %, diffusion coefficient increases. However, at 1.5 wt%, nanoclay agglomeration limits any further increase in surface area, causing a decrease in saturation moisture content.

The moisture absorption behavior of epoxy and epoxy clay nanocomposites when immersed in artificial seawater at 28 °C is shown in Fig. 10, wherein the scatter plot of M_t/M_∞ versus $\sqrt{t}$ is fit by Fick's law. The diffusion coefficient obtained by curve fitting and saturation moisture uptake obtained from experimentation is given in Table 3. Adjusted R-square, SSE and RMSE values are given in Table 4.

In case of artificial seawater immersion, the same trend as distilled water immersion is observed as far as effect of amount of nanoclay on diffusion coefficient is concerned. However, the values are higher for artificial seawater diffusion. This is because, when distilled water enters, it first interacts with the cations in the nanoclay and then move on to polymer. But in the case of artificial seawater, there is no such interaction and the seawater directly moves into the polymer. Hence, diffusion coefficient is observed to be higher in the case of artificial seawater [37]. The phenomenon of artificial sea water not interacting with cations in the surface of nanoclay, makes the diffusion only dependent on dispersion of nanoclay or nanoclay structure. Since there is better dispersion of nanoclay, the saturation moisture uptake reduces with increase in amount of nanoclay. However, because of greater degree of agglomeration at higher nanoclay loadings, the saturation moisture uptake has increased when nanoclay was increased from 1 to 1.5 wt%. The agglomeration behavior is observed for 1 wt% in AFM images and XRD spectra and hence much bigger agglomeration is expected for 1.5 wt% nanoclay loadings.

The variation of diffusion coefficients in distilled water and artificial seawater at 28 °C for different nanoclay content with their standard deviation showing the repeatability of the results are shown in Fig. 11.

The experimental data was curve fit using two models-Fick's and Langmuir. The diffusion coefficient obtained using Langmuir model was observed to be highest as it was observed elsewhere [38, 39]. The adjusted R-square values when Langmuir model was fit was higher than Fick's model. Therefore, it can be ascertained that Langmuir model accounts for the non-linearity in the experimental data and hence approximates the data better than Fick's law [40, 41]. The scatter

plot along with curve fit representing Langmuir model is shown in Figs. 12 and 13 for distilled water and artificial seawater respectively. The adjusted R-square, SSE and RMSE obtained by fitting Langmuir model is given in Table 5. The diffusion coefficient, γ (probability of mobile molecules getting bound) and α (probability of bound molecules becoming mobile) are given in Table 6.

Moisture absorption studies on neat epoxy and epoxy clay nanocomposites at 38 °C

It was intended to compare the change in diffusion coefficient when temperature is increased. Therefore, only one medium i.e., artificial seawater was chosen and nanoclay was varied only till 1 wt%. The experimental scatter plots were fit by only Fick's Law is shown in Fig. 14. The comparison of diffusion coefficients is given in Table 7. It is observed from the Table 7 that due to higher temperatures, the diffusion coefficient is higher. At higher temperatures rate of moisture diffusion, hydrolysis, chemical degradation, blistering, oxidation and leaching of small molecules is higher [42].

SEM–EDX analysis of epoxy clay nanocomposite post immersion

The elemental composition of neat epoxy post artificial seawater immersion at 28 °C is shown in Fig. 15. It is observed in neat epoxy that, carbon (C) is the major element, followed by oxygen (O), sodium (Na), chlorine (Cl) and magnesium (Mg).
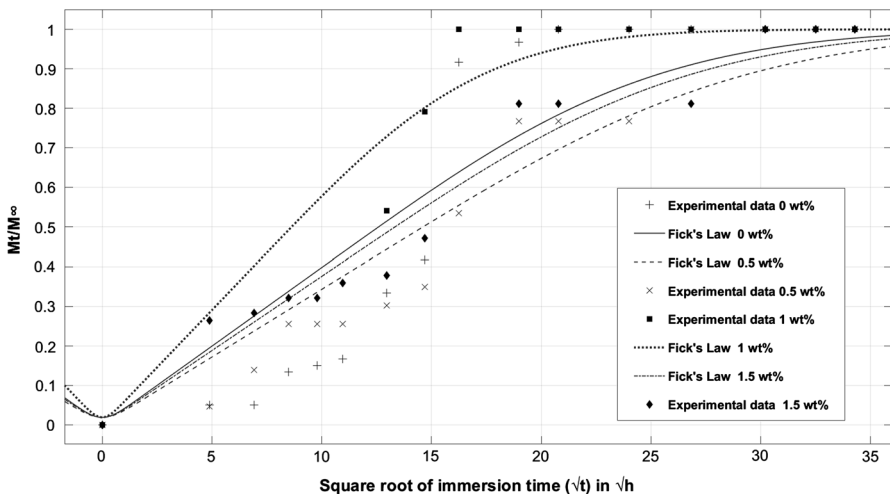
Fig. 10 Experimental data scatter plot of M_t/M_∞ versus $\sqrt{t}$ of samples immersed in artificial seawater at 28 °C along with Fick's law fit curve
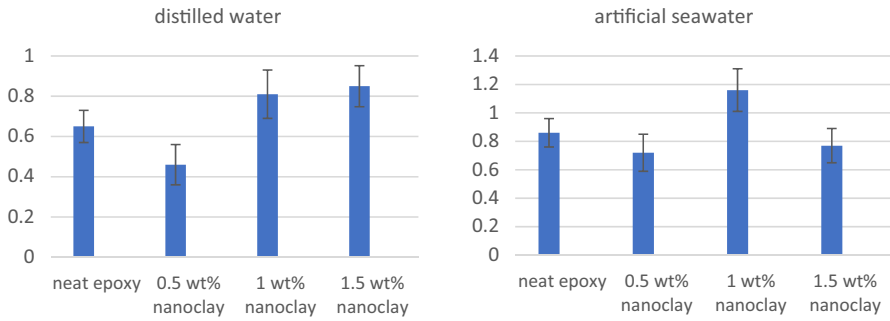
Fig. 11 Variation of diffusion coefficient with change in nanoclay content for distilled water and artificial seawater (diffusion coefficient (mm2/s)×107)

Carbon and oxygen correspond to the organic epoxy polymer and remaining elements corresponds to the penetrated salts from the artificial seawater.

In epoxy clay nanocomposite containing 1.5 wt% nanoclay, other than the above elements, nitrogen (N), aluminum (Al), silicon (Si), potassium (K), calcium (Ca) and iron (Fe) are also present (Fig. 16, 17). Al and Si represent the presence of nanoclay layers. N represents the presence of amine in surface modification of nanoclay [6]. K, Ca and Fe correspond to the cations still present even after surface modification; therefore, some hydrophilicity will still be present in nanoclay. To be assured of this, EDX analysis was also carried out for epoxy clay nanocomposite immersed in distilled water. As distilled water do not contain ions, the cations detected in the sample correspond to the cations of the nanoclay (Fig. 18).
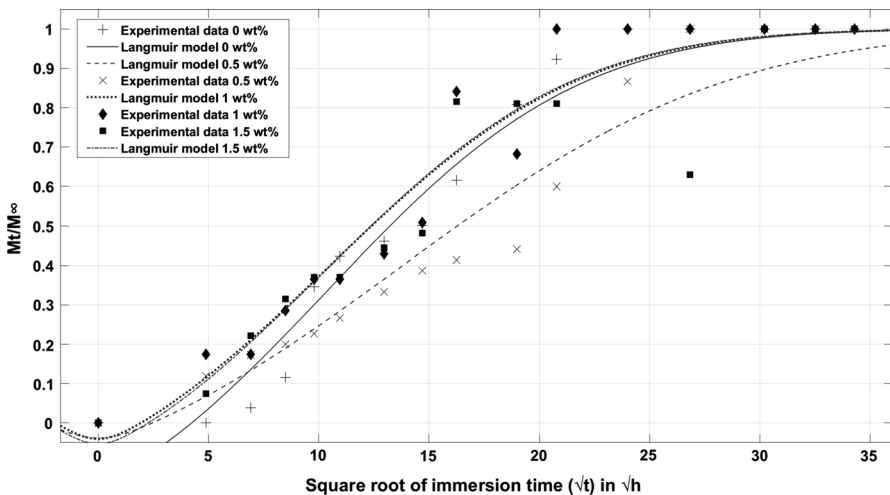
Fig. 12 Experimental data scatter plot of M_t/M_∞ versus $\sqrt{t}$ of samples immersed in distilled water at 28 °C along with Langmuir model fit curve. (nanoclay varied from 0 to 1.5 wt% in epoxy)
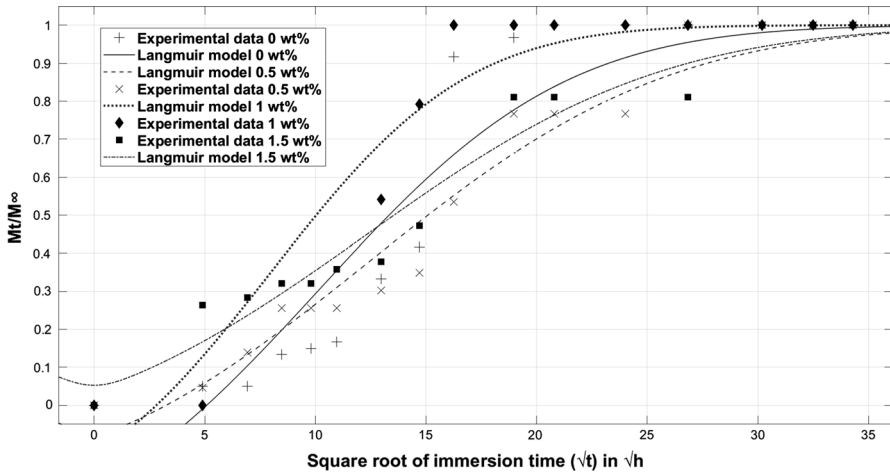
Fig. 13 Experimental data scatter plot of M_t/M_∞ versus $\sqrt{t}$ of samples immersed in artificial seawater at 28 °C along with Langmuir model fit curve

FTIR analysis post immersion

The FTIR spectra from Figs. 19, 20, 21 presents comparisons between dry and wet samples of neat epoxy, epoxy clay nanocomposite containing 0.5 and 1 wt% nanoclay. The effect of distilled water immersion on saturation moisture uptake was investigated by studying the hydroxyl group (OH) peak at the range of 3317–3373 cm^{-1} [34]. The FTIR spectra comparison shows that, the transmittance in the wavenumber region 3317–3373 decreases because the presence of water in the specimen hinders the transmittance of infrared light. Further, Fig. 22 presents comparison of wet samples, epoxy, and epoxy clay nanocomposites, wherein effect of nanoclay incorporation on saturation moisture uptake is investigated qualitatively. It can be noted that, the transmittance in the region of interest decreases as nanoclay content increases. This goes well with the water absorption gravimetric data presented in Table 3, which conveys that as nanoclay increases, the saturation moisture uptake also increases.

Conclusions

The moisture absorption behaviour of neat epoxy and epoxy clay nanocomposites were studied in distilled and artificial seawater at 28 and 38 °C. Moisture absorption experimental data was fit numerically by Fick's law and Langmuir model and diffusion coefficient was calculated from it. The results indicate that the nanocomposites perform better when nanoclay is 0.5 wt% in distilled water. Addition of 0.5 wt% nanoclay decreased the diffusivity or diffusion coefficient. Among the two models, Langmuir model fit the experimental data better and give higher diffusion coefficient because it accounts for presence of bound and mobile diffusing molecules. The

Table 5 Adjusted R square, SSE and RMSE values obtained after Langmuir curve fitting

	Adjusted R-square		SSE		RMSE	
	Distilled water	Artificial seawater	Distilled water	Artificial seawater	Distilled water	Artificial seawater
Neat epoxy	0.96	1.22	0.19	0.29	0.11	0.15
Epoxy clay nanocomposite (0.5 wt% nanoclay)	0.94	0.95	0.12	0.06	0.09	0.07
Epoxy clay nanocomposite (1 wt% nanoclay)	0.94	1.27	0.14	0.11	0.10	0.09
Epoxy clay nanocomposite (1.5 wt% nanoclay)	0.81	0.94	0.36	0.06	0.17	0.07

increase in temperature raised the diffusion coefficient; rate of moisture diffusion, hydrolysis, chemical degradation, blistering, oxidation and leaching of small molecules is higher at higher temperatures.

AFM analysis revealed the effect of nanoclay on surface roughness. Surface roughness increased with increase in nanoclay. The tendency of nanoclay to migrate to the surface caused the increase in surface roughness. The topography and phase images from AFM analysis also indicate formation of bigger nanoclay agglomerations at nanoclay loading of 1 wt% which is also the reason why diffusion coefficient is lower at nanoclay loading of 0.5 wt%. XRD revealed exfoliated structure of nanoclay at 0.5 wt% and mixture of intercalated and exfoliated structure at 1 wt%. FTIR analysis of dry specimens provided information about the presence of various chemical bonds in nanoclay and epoxy clay nanocomposite specimens, which directed in determining the reaction mechanism in the formation of epoxy clay nanocomposite. FTIR analysis of wet specimens helped in analyzing how transmittance decreased relative to dry specimens. The increase in saturation moisture uptake with increase in nanoclay content for distilled water immersed specimens at 28 °C, is well supported by the FTIR spectra of wet specimens. The transmittance in the region of wavenumber 3317–3373 cm^{-1} reveals the presence of absorbed water molecules. With increase in nanoclay content, transmittance decreased, because higher the

Table 6 Diffusion coefficient, γ and α obtained by Langmuir curve fitting

|	Diffusion coefficient $(mm^2/s) \times 10^7$		$\gamma \times 10^3$		$\alpha \times 10^3$	
	Distilled water	Artificial seawater	Distilled water	Artificial seawater	Distilled water	Artificial seawater
Neat epoxy	0.91	1.22	4.34	4.45	3.175	2.88
Epoxy clay nanocomposite (0.5 wt% nanoclay)	0.60	0.83	2.41	2.97	2.16	2.50
Epoxy clay nanocomposite (1 wt% nanoclay)	1.04	1.90	4.19	7.25	3.75	5.63
Epoxy clay nanocomposite (1.5 wt% nanoclay)	1.23	0.94	4.34	2.78	3.78	3.01
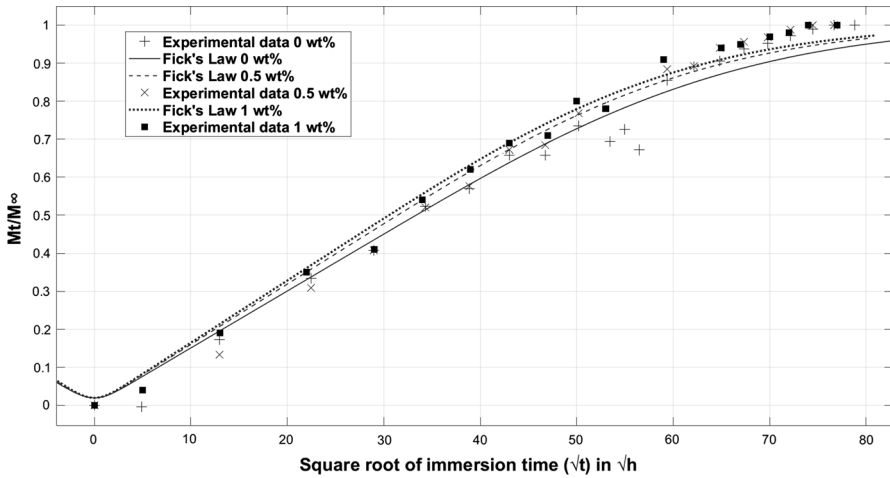
Fig. 14 Experimental data scatter plot of M_t/M_∞ versus $\sqrt{t}$ of samples immersed in artificial seawater at 38 °C along with Fick's model fit curve. (nanoclay varied from 0 to 1 wt% in epoxy)

Table 7 Diffusion coefficient comparison at different temperatures		Diffusion coefficient (mm²/s)×10^7 28 °C	Diffusion coefficient (mm²/s)×10^7 38 °C
	Neat epoxy	0.86	2.77
	Epoxy clay nanocomposite (0.5 wt% nano-clay)	0.64	1.98
	Epoxy clay nano-composite (1 wt% nanoclay)	1.84	2.19
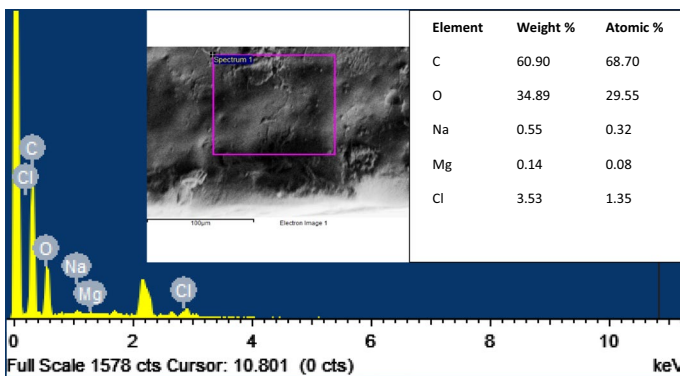
Fig. 15 EDX image of neat epoxy (0 wt% nanoclay) post artificial seawater immersion
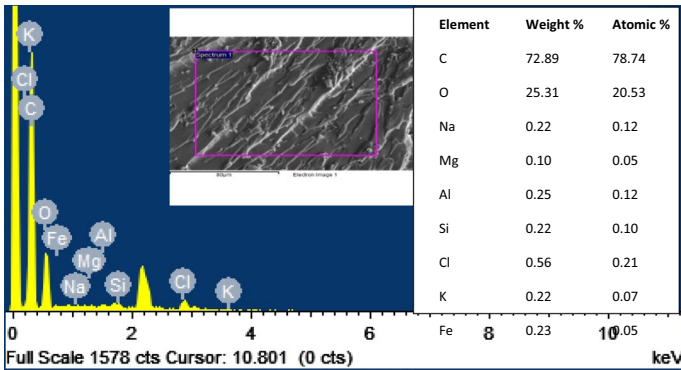
Element	Weight %	Atomic %
C	72.89	78.74
O	25.31	20.53
Na	0.22	0.12
Mg	0.10	0.05
Al	0.25	0.12
Si	0.22	0.10
Cl	0.56	0.21
K	0.22	0.07
Fe	0.23	0.05

Full Scale 1578 cts Cursor: 10.801 (0 cts)

Fig. 16 EDX image of epoxy clay nanocomposite (1.5 wt% nanoclay) post artificial seawater immersion

Element	Weight %	Atomic %
C	65.90	72.63
N	5.38	5.08
O	26.12	21.61
Mg	0.09	0.05
K	0.25	0.09
Ca	0.00	0.00
Fe	2.27	0.54

Full Scale 1578 cts Cursor: 10.801 (0 cts)
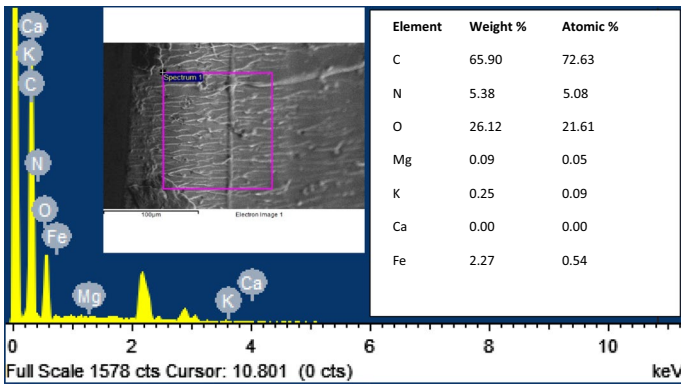
Fig. 17 EDX image of epoxy clay nanocomposite (1.5 wt% nanoclay) post artificial seawater immersion at a different location in the sample

Element	Weight %	Atomic %
C	81.31	85.43
O	18.24	14.39
Na	0.01	0.01
Mg	0.02	0.01
Al	0.08	0.04
Si	0.08	0.04
Cl	0.19	0.07
K	0.04	0.01
Ca	0.03	0.01

Full Scale 1850 cts Cursor: 0.000
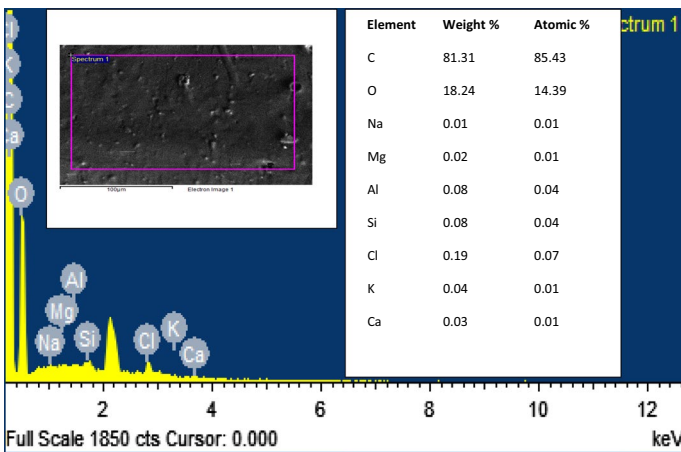
Fig. 18 EDX image of epoxy clay nanocomposite (1.5 wt% nanoclay) post distilled water immersion
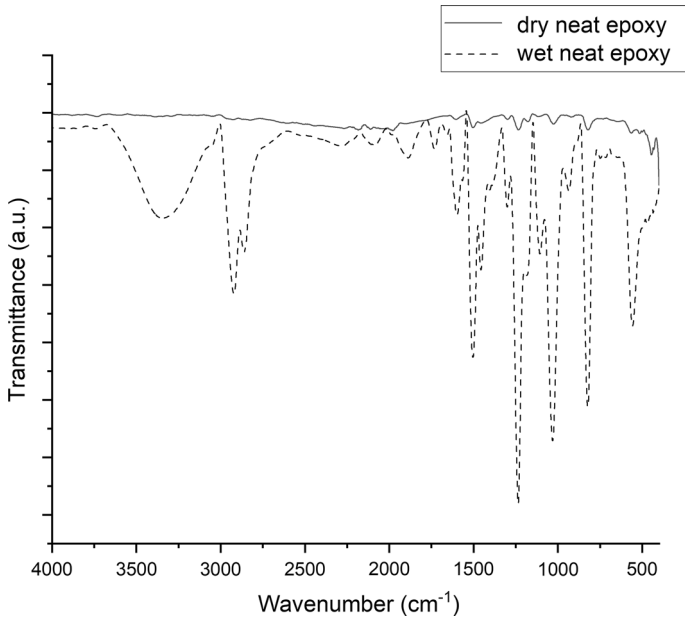
Fig. 19 FTIR spectra comparison of dry and wet neat epoxy
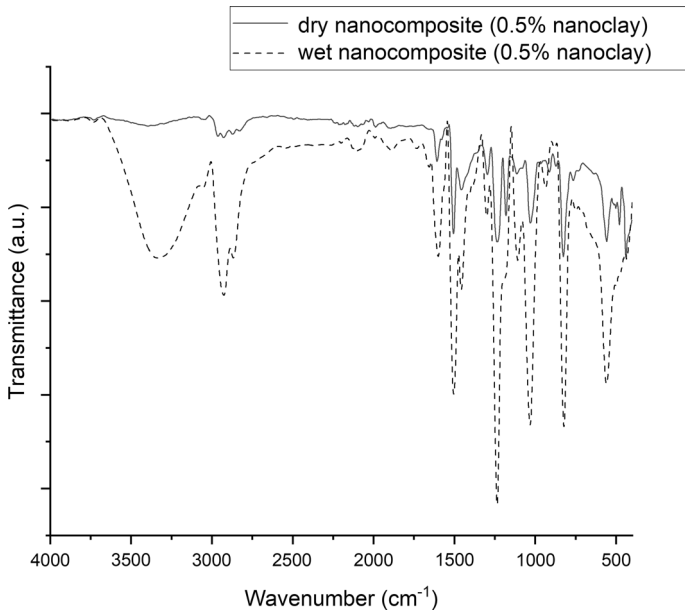
Fig. 20 FTIR spectra comparison of dry and wet epoxy clay nanocomposite containing 0.5 wt% nanoclay
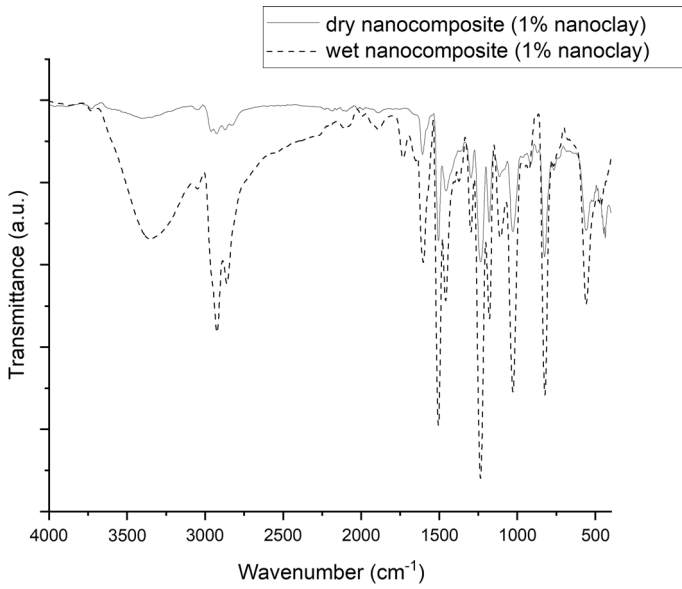
Fig. 21 FTIR spectra comparison of dry and wet epoxy clay nanocomposite containing 1 wt% nanoclay
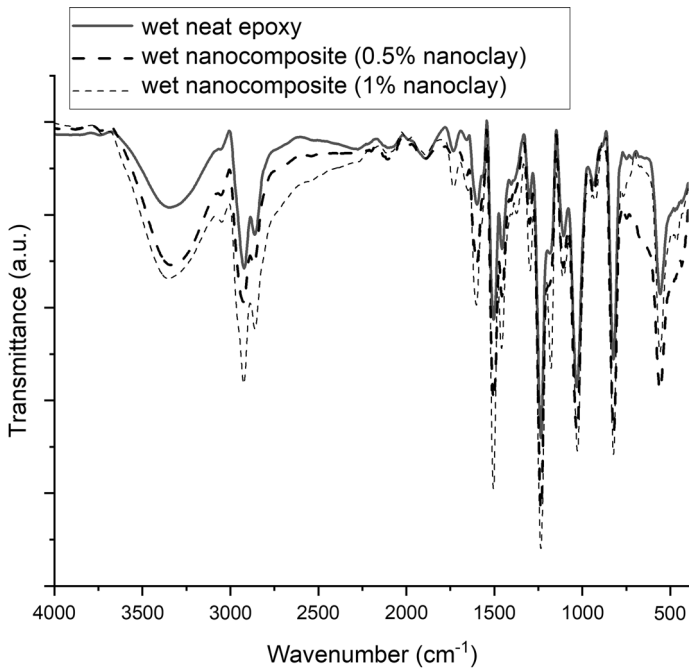
Fig. 22 FTIR spectra comparison of wet epoxy and epoxy clay nanocomposites

saturation moisture uptake, greater is the hindrance to transmission of infrared light. The SEM–EDX analysis revealed the presence of penetrated artificial seawater salts and helped in proving the hydrophilic nature of nanoclay still present in the organo-modified nanoclay, which is the reason for higher diffusion coefficient of nanocomposites in artificial seawater when compared with distilled water medium.

Declarations

Conflict of interest The authors declare that they have no known conflict of interest or personal relationships that could have influenced the work reported in this paper.

References

1. Radhamani AV, Lau HC, Ramakrishna S (2020) Nanocomposite coatings on steel for enhancing the corrosion resistance: a review. J Compos Mater 54:681–701. https://doi.org/10.1177/0021998319857807

2. Aghili M, Yazdi MK, Ranjbar Z, Jafari SH (2021) Anticorrosion performance of electro-deposited epoxy/amine functionalized graphene oxide nanocomposite coatings. Corros Sci 179:109143. https://doi.org/10.1016/j.corsci.2020.109143

3. Rafiq A, Merah N (2019) Nanoclay enhancement of flexural properties and water uptake resistance of glass fiber-reinforced epoxy composites at different temperatures. J Compos Mater 53:143–154. https://doi.org/10.1177/0021998318781220

4. Rao YQ, Liu A, O'Connell K (2018) Barrier properties and structure of liquid crystalline epoxy and its nanocomposites. Polymer (Guildf) 142:109–118. https://doi.org/10.1016/j.polymer.2018.03.027

5. Merachtsaki D, Xidas P, Giannakoudakis P, Triantafyllidis K, Spathis P (2017) Corrosion protection of steel by epoxy-organoclay nanocomposite coatings. Coatings 7:84. https://doi.org/10.3390/coatings7070084

6. Azeez AA, Rhee KY, Park SJ, Hui D (2013) Epoxy clay nanocomposites - processing, properties and applications: a review. Compos Part B Eng 45:308–320. https://doi.org/10.1016/j.compositesb.2012.04.012

7. Xiao GZ, Delamar M, Shanahan MER (1997) Irreversible interactions between water and DGEBA/DDA epoxy resin during hygrothermal aging. J Appl Polym Sci 65:449–458. https://doi.org/10.1002/(sici)1097-4628(19970718)65:3%3c449::aid-app4%3e3.0.co;2-h

8. Legghe E, Aragon E, Bélec L, Margaillan A, Melot D (2009) Correlation between water diffusion and adhesion loss: study of an epoxy primer on steel. Prog Org Coat 66:276–280. https://doi.org/10.1016/j.porgcoat.2009.08.001

9. Krauklis AE, Gagani AI, Echtermeyer AT (2018) Hygrothermal aging of amine epoxy: reversible static and fatigue properties. Open Eng 8:447–454. https://doi.org/10.1515/eng-2018-0050

10. García C, Fittipaldi M, Grace LR (2015) Epoxy/montmorillonite nanocomposites for improving aircraft radome longevity. J Appl Polym Sci 132:1–9. https://doi.org/10.1002/app.42691

11. Al-Qadhi M, Merah N (2015) Mechanical and physical properties of polymer-based nanocomposites containing different types of clay. Polym Compos 36:1998–2007. https://doi.org/10.1002/pc.23109

12. Nandiyanto ABD, Oktiani R, Ragadhita R (2019) How to read and interpret ftir spectroscope of organic material. Indones J Sci Technol 4:97–118. https://doi.org/10.17509/ijost.v4i1.15806

13. Karami Khorramabadi M (2020) Theoretical predictions on mechanical properties of functionally graded epoxy/clay nanocomposites. ADMT J 13:31–37

14. Annappa AR, Shivaramu PD (2021) Spectral characterization of morphological structure of organomodified montmorillonite clay-based epoxy nanocomposite. Int J Polym Anal Charact 26:471–485. https://doi.org/10.1080/1023666X.2021.1908031

15. Thipperudrappa S, Hiremath A, Kurki Nagaraj B (2021) Synergistic effect of ZnO and TiO$_2$ nanoparticles on the thermal stability and mechanical properties of glass fiber-reinforced LY556 epoxy composites. Polym Compos 42:4831–4844. https://doi.org/10.1002/pc.26193

16. ASTM D570 (2014) Standard test method for water absorption of plastics. ASTM Stand 98:25–28. https://doi.org/10.1520/D0570-98R18.2

17. Ataeefard M, Moradian S (2011) Surface properties of polypropylene/organoclay nanocomposites. Appl Surf Sci 257:2320–2326. https://doi.org/10.1016/j.apsusc.2010.09.096

18. James Jose A, Chacko F, Wilson R, Alagar M (2020) Development and characterization of organoclay filled polyetherimide nanocomposites for anticorrosive coatings. Mater Today Proc 41:490–497. https://doi.org/10.1016/j.matpr.2020.05.232

19. Darmiani E, Rashed GR, Zaarei D, Danaee I (2013) Synergistic effects of montmorillonite/cerium nitrate additives on the corrosion performance of epoxy-clay nanocomposite coatings. Polym Plast Technol Eng 52:980–990. https://doi.org/10.1080/03602559.2013.763373

20. Fatemi Khadar P, Maghsoud Z, Dashti A (2020) Synthesis, characterization, and dynamic-mechanical properties of styrene-acrylate/nanoclay interpenetrating polymer network. Polym Compos 41:982–993. https://doi.org/10.1002/pc.25429

21. Thomas S, Shumilova AA, Kiselev EG, Baranovsky SV, Vasiliev AD, Nemtsev IV, Kuzmin AP, Sukovatyi AG, Avinash RP, Volova TG (2020) Thermal, mechanical and biodegradation studies of biofiller based poly-3-hydroxybutyrate biocomposites. Int J Biol Macromol 155:1373–1384. https://doi.org/10.1016/j.ijbiomac.2019.11.112

22. Kumar M, Arun S, Upadhyaya P, Pugazhenthi G (2015) Properties of PMMA/clay nanocomposites prepared using various compatibilizers. Int J Mech Mater Eng. https://doi.org/10.1186/s40712-015-0035-x.10.1186/s40712-015-0035-x

23. Lobato-Aguilar H, Uribe-Calderón JA, Herrera-Kao W, Duarte-Aranda S, Baas-López JM, Escobar-Morales B, Cauich-Rodríguez JV, Cervantes-Uc JM (2018) Synthesis, characterization and chlorhexidine release from either montmorillonite or palygorskite modified organoclays for antibacterial applications. J Drug Deliv Sci Technol 46:452–460. https://doi.org/10.1016/j.jddst.2018.06.007

24. Deka BK, Maji TK (2010) Effect of coupling agent and nanoclay on properties of HDPE, LDPE, PP, PVC blend and phargamites karka nanocomposite. Compos Sci Technol 70:1755–1761. https://doi.org/10.1016/j.compscitech.2010.07.010

25. Bhadran B, Vijayan D, George N, Julie Chandra CS, Sabura Begum PM, Joseph R (2018) Reinforcing effect of organoclay in nitrile rubber - effect of mill mixing and latex stage mixing. Appl Clay Sci 165:91–102. https://doi.org/10.1016/j.clay.2018.07.027

26. Chan ML, Lau KT, Wong TT, Cardona F (2011) Interfacial bonding characteristic of nanoclay/polymer composites. Appl Surf Sci 258:860–864. https://doi.org/10.1016/j.apsusc.2011.09.016

27. Pandit R, Lach R, Grellmann W, Michler GH, Henning S, Saiter JM, Berkessel A, Adhikari R (2020) Chemical modification of SBS star block copolymer for templating nanostructures in epoxy resin blends. Mater Today Proc 29:1156–1160. https://doi.org/10.1016/j.matpr.2020.05.398

28. Zhang W, Li X, Yang R (2011) Pyrolysis and fire behaviour of epoxy resin composites based on a phosphorus-containing polyhedral oligomeric silsesquioxane (DOPO-POSS). Polym Degrad Stab 96:1821–1832. https://doi.org/10.1016/j.polymdegradstab.2011.07.014

29. Nikolic G, Zlatkovic S, Cakic M, Cakic S, Lacnjevac C, Rajic Z (2010) Fast fourier transform IR characterization of epoxy GY systems crosslinked with aliphatic and cycloaliphatic EH polyamine adducts. Sensors 10:684–696. https://doi.org/10.3390/s100100684

30. Singh KP, Singh A, Kumar N, Tripathi DN (2020) Morphological features, dielectric and thermal properties of epoxy–copper cobaltite nanocomposites: preparation and characterization. Bull Mater Sci. https://doi.org/10.1007/s12034-020-02092-9

31. Shanmugharaj AM, Ryu SH (2012) Study on the effect of aminosilane functionalized nanoclay on the curing kinetics of epoxy nanocomposites. Thermochim Acta 546:16–23. https://doi.org/10.1016/j.tca.2012.07.026

32. Huskić M, Žigon M, Ivanković M (2013) Comparison of the properties of clay polymer nanocomposites prepared by montmorillonite modified by silane and by quaternary ammonium salts. Appl Clay Sci 85:109–115. https://doi.org/10.1016/j.clay.2013.09.004

33. Firdosh S, Narasimha Murthy HN, Angadi G, Raghavendra N (2018) Investigation of water absorption characteristics of nano-gelcoat for marine application. Prog Org Coat 114:173–187. https://doi.org/10.1016/j.porgcoat.2017.10.004

34. Alamri H, Low IM (2012) Effect of water absorption on the mechanical properties of nano-filler reinforced epoxy nanocomposites. Mater Des 42:214–222. https://doi.org/10.1016/j.matdes.2012.05.060

35. Zabihi O, Ahmadi M, Nikafshar S, Chandrakumar Preyeswary K, Naebe M (2018) A technical review on epoxy-clay nanocomposites: structure, properties, and their applications in fiber reinforced composites. Compos Part B Eng 135:1–24. https://doi.org/10.1016/j.compositesb.2017.09.066

36. Abacha N, Kubouchi M, Sakai T (2009) Diffusion behavior of water in polyamide 6 organoclay nanocomposites. Express Polym Lett 3:245–255. https://doi.org/10.3144/expresspolymlett.2009.31

37. Bal S, Saha S (2017) Effect of sea and distilled water conditioning on the overall mechanical properties of carbon nanotube/epoxy composites. Int J Damage Mech 26:758–770. https://doi.org/10.1177/1056789515615184

38. Liu W, Hoa SV, Pugh M (2008) Water uptake of epoxy-clay nanocomposites: experiments and model validation. Compos Sci Technol 68:2066–2072. https://doi.org/10.1016/j.compscitech.2007.07.024

39. Agwa MA, Taha I, Megahed M (2017) Experimental and analytical investigation of water diffusion process in nano-carbon/alumina/silica filled epoxy nanocomposites. Int J Mech Mater Des 13:607–615. https://doi.org/10.1007/s10999-016-9335-4

40. Sridhar R, Narasimha Murthy HN, Karthik B, Vishnu Mahesh KR, Krishna M, Ratna P (2014) Moisture diffusion through nanoclay/vinylester processed using twin-screw extrusion. J Vinyl Addit Technol 20:152–159. https://doi.org/10.1002/vnl.21367

41. Raghavendra N, Narasimha Murthy HN, Firdosh S, Sridhar R, Angadi G, Vishnu Mahesh KR, Krishna M (2016) Moisture diffusion through (hexadecyltrimethylammonium bromide - Indian bentonite)/(vinylester) nanocomposites in artificial seawater and demineralized water. J Vinyl Addit Technol 22:441–451. https://doi.org/10.1002/vnl.21463

42. Chakraverty AP, Mohanty UK, Mishra SC, Satapathy A (2015) Sea water ageing of GFRP composites and the dissolved salts. IOP Conf Ser Mater Sci Eng 75:012029. https://doi.org/10.1088/1757-899X/75/1/012029

Authors and Affiliations

K. Muralishwara[1] · **Y. N. Sudhakar**[2] · **U. Achutha Kini**[1] ·
Sathyashankara Sharma[1] · **B. M. Gurumurthy**[1]

✉ U. Achutha Kini
achutha.kini@manipal.edu

[1] Department of Mechanical and Industrial Engineering, Manipal Institute of Technology,
Manipal Academy of Higher Education, Manipal, Karnataka 576104, India

[2] Department of Chemistry, Manipal Institute of Technology, Manipal Academy of Higher
Education, Manipal, Karnataka 576104, India